A vector-based method for bank-material tracking in coupled models of meandering and landscape evolution

Ajay B. S. Limaye[1] and Michael P. Lamb[1]

Received 13 May 2013; revised 30 October 2013; accepted 31 October 2013.

[1] Sinuous channels commonly migrate laterally and interact with banks of different strengths—an interplay that links geomorphology and life and shapes diverse landscapes from the seafloor to planetary surfaces. To investigate feedbacks between meandering rivers and landscapes over geomorphic timescales, numerical models typically represent bank properties using grids; however, this approach produces results inherently dependent on grid resolution. Herein we assess existing techniques for tracking landscape and bank-strength evolution in numerical models of meandering channels and show that grid-based models implicitly include unintended thresholds for bank migration that can control simulated landscape evolution. Building on stratigraphic modeling techniques, we develop a vector-based method for land surface- and subsurface-material tracking that overcomes the resolution-dependence inherent in grid-based techniques by allowing high-fidelity representation of bank-material properties for curvilinear banks and low channel lateral migration rates. We illustrate four specific applications of the new technique: (1) the effect of resistant mud-rich deposits in abandoned meander cutoff loops on meander belt evolution; (2) the stratigraphic architecture of aggrading, alluvial meandering channels that interact with cohesive-bank and floodplain material; (3) the evolution of an incising, meandering river with mixed bedrock and alluvial banks within a confined bedrock valley; and (4) the effect of a bank-height dependent lateral-erosion rate for a meandering river in an aggrading floodplain. In all cases the vector-based approach overcomes numerical artifacts with the grid-based model. Because of its geometric flexibility, the vector-based material tracking approach provides new opportunities for exploring the coevolution of meandering rivers and surrounding landscapes over geologic timescales.

Citation: Limaye, A. B. S., and M. P. Lamb (2013), A vector-based method for bank-material tracking in coupled models of meandering and landscape evolution, *J. Geophys. Res. Earth Surf.*, *118*, doi:10.1002/2013JF002854.

1. Introduction

[2] Meandering channels traverse, erode, and construct landscapes in a wide variety of planetary environments. These include river channels in high-relief mountain landscapes [e.g., *Stark et al.*, 2010] and lowland plains [e.g., *Bridge*, 2003], tidal channels [e.g., *Fagherazzi et al.*, 1999] and deltas [e.g., *Hudson and Kesel*, 2000], subglacial [e.g., *Weertman*, 1972] and supraglacial channels [e.g., *Parker*, 1975], channels formed by lava [e.g., *Greeley et al.*, 1998], and submarine channels formed by turbidity currents [e.g., *Abreu et al.*, 2003]. In all of these environments, channel lateral migration is influenced by bank strength, and through erosion and deposition, there is a rich interplay between channel migration, bank-material strength, and landscape evolution. Bank interaction holds fundamental implications for a number of topics, including flood hydraulics [*Smith*, 1978; *Shiono et al.*, 1999] and the geomorphic expression of climate [*Blum and Tornqvist*, 2000; *Stark et al.*, 2010]. Because vegetation influences bank strength and the stability of sinuous channels [*Braudrick et al.*, 2009], bank strength is also central to the topographic signature of life [*Dietrich and Perron*, 2006] and the development of land plants [*Davies and Gibling*, 2010], as well as stream restoration [*Kondolf*, 2006] and ecology [*Trush et al.*, 2000]. Moreover, an understanding of channel-bank interactions is needed to unravel climatic conditions and material properties for channel meandering on Mars, Venus, the Moon, [*Komatsu and Baker*, 1996] and Titan [*Burr et al.*, 2013].

[3] A variety of factors can influence bank strength including lithology or soil type, vegetation, and susceptibility to weathering from freeze-thaw and wet-dry cycles [*Howard*, 1992; *Montgomery*, 2004]. Differences in bank strength in turn exert first-order controls on channel kinematics in meandering rivers. For example, valley confinement can distort smoothly curving meander bends into sharp bends at valley walls [*Lewin*, 1976; *Lewin and Brindle*, 1977; *Allen*, 1982]. Meandering rivers deposit sediments on the trailing bank and overbank which typically have different strength properties than

[1]Division of Geological and Planetary Sciences, California Institute of Technology, Pasadena, California, USA.

Corresponding author: A. B. S. Limaye, Division of Geological and Planetary Sciences, California Institute of Technology, MC 170-25, 1200 E. California Blvd., Pasadena, CA 91125, USA. (ajay@caltech.edu)

2169-9003/13/10.1002/2013JF002854

the preexisting sediment or rock substrate—for example, when erosion-resistant, fine-grained sediment accumulates in abandoned meander loops [*Fisk*, 1947; *Ikeda*, 1989; *Thorne*, 1992].

[4] To model meandering river and landscape evolution, there is a need to accurately couple channel migration with bank-material evolution. Relatively short-timescale models have detailed the influence of stochastic floodplain bank strength on alluvial channel geometry [*Güneralp and Rhoads*, 2011; *Motta et al*., 2012b; *Posner and Duan*, 2012]. Forward models of river meandering over geologic timescales have generated predictions for the planform evolution meander belts [*Howard*, 1996; *Sun et al*., 1996; *Camporeale et al*., 2005; *Karssenberg and Bridge*, 2008], feedbacks between channel migration and floodplain deposition [*Howard*, 1996; *Sun et al*., 1996, 2001], the development of river terraces by incising channels [*Finnegan and Dietrich*, 2011], tectonic uplift influences on channel migration rates [*Lancaster*, 1998], and stratigraphic development in subaerial [*Clevis et al*., 2006; *Karssenberg and Bridge*, 2008] and submarine environments [*Sylvester et al*., 2011]. Despite this diversity of work, incorporating channel migration in landscape evolution models poses continuing challenges. River banks are commonly steep and mobile, and representing their geometry and erodibility with a grid in numerical models can be problematic [*Tucker and Hancock*, 2010]. While techniques for evolving channel centerlines have been critically assessed [*Crosato*, 2007], to our knowledge, no systematic sensitivity tests have been performed for models that represent bank strength in environments influenced by channel migration.

[5] Herein we present a novel framework for tracking the interaction of a migrating channel and its banks in a landscape evolution model. Section 2 establishes the goal of this study: to robustly couple meandering models to a framework for tracking bank-material properties over the temporal and spatial scales of interest for landscape evolution modeling. Section 3 reviews existing approaches to modeling landscape evolution with channel migration and shows that a common, grid-based framework for bank-material tracking can yield results highly sensitive to grid resolution. In section 4, we present a new, vector-based framework for modeling the coevolution of a meandering river and its surroundings. We also compare results from grid- and vector-based simulations. In section 5, we explore the implications of vector-based bank-material tracking for case studies involving subaerial meandering rivers. These examples include the evolution of meander belts with resistant mud-filled abandoned meander cutoffs, the stratigraphic architecture of channel deposits for aggradational meandering rivers with variable bank strength, valley width evolution caused by an incising, meandering river with mixed alluvial and bedrock banks, and bank-height dependent channel migration across an aggrading floodplain. We discuss advantages and disadvantages of grid- and vector-based approaches to bank-material tracking in section 6 and present conclusions in section 7.

2. Modeling Goal

[6] Our modeling goal is to develop a numerical framework that can be used to track bank-material properties in a landscape evolution model of a meandering river in the absence of grid-resolution dependencies. In their review of modeling approaches to alluvial river evolution, *Van De Wiel et al*. [2011] identified three principal fronts for progress in modeling meandering rivers and landscape evolution: (1) conceptual: relating to understanding underlying physical processes; (2) structural: relating to algorithms and mathematical formulations within models; and (3) computational resources. Accurate tracking of bank-material properties represents a fundamental structural component of channel migration models because bank strength strongly influences the channel trajectory [*Seminara*, 2006]. In this way, numerical artifacts in tracking bank strength may shape simulated landscapes in subtle but fundamental ways, obscuring the links between physical models and natural process and form [*Dietrich et al*., 2003].

[7] Here we make no contributions to modeling river channel sediment transport and hydrodynamics apart from the interaction between the channel and the evolving landscape. A wide range of channel lateral migration models exist, and they vary considerably in complexity depending on the spatial and temporal scales of the intended application. Some detailed, mathematical models resolve short-term evolution of the left and right bank positions independently and include explicit physical models of sediment transport and bank failure [e.g., *Osman and Thorne*, 1988; *Nagata et al*., 2000; *Darby*, 2002; *Shimizu*, 2002; *Duan and Julien*, 2010; *Parker et al*., 2011; *Motta et al*., 2012a] but are computationally intensive to implement. More commonly, local feedbacks between cutbank erosion and point-bar growth are approximated as continuous processes [*Seminara*, 2006], and channel width is assumed to be constant [*Parker et al*., 2011], consistent with field observations [e.g., *Leopold and Wolman*, 1957; *Parker et al*., 2011]. Some channel models explicitly represent hydraulics and bed topography [e.g., *Blondeaux and Seminara*, 1985; *Johannesson and Parker*, 1989], while others employ physically motivated rules [e.g., *Howard and Knutson*, 1984; *Lancaster and Bras*, 2002] to predict local bank migration rates. Computational costs increase with the complexity of the hydraulic and morphodynamic models, so given our interest in landscape evolution over geomorphic timescales, herein we employ a relatively simple model (constant channel width, rule based) that has been shown to produce realistic meandering to represent lateral migration [*Howard and Knutson*, 1984; *Howard and Hemberger*, 1991]. We use this model as the driver of landscape evolution and focus our efforts on properly representing bank-material properties and topography. The landscape-evolution framework we develop is generic, however, so that it can be used in conjunction with a wide range of models for meandering river channels [e.g., *Johannesson and Parker*, 1989; *Zolezzi and Seminara*, 2001].

3. Grid-Based Approaches to Bank-Material Tracking

[8] We begin this section by reviewing grid-based models for tracking bank-material properties. Second, we introduce a typical setup for grid-based erodibility tracking. Third, we show model results from our own grid-based simulations to illustrate shortcomings with this technique. This leads us to introduce the new vector-based technique in section 4.

3.1. Review of Existing Grid-Based Models

[9] Existing approaches to bank-material tracking over geomorphic timescales all utilize a grid—regularly spaced and fixed or irregularly spaced and deformable. Two-dimensional

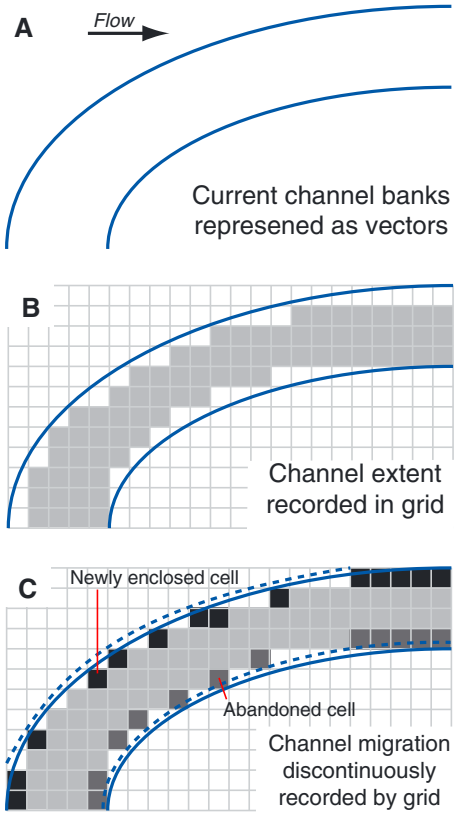

Figure 1. A commonly used technique for representing bank-material properties in models of landscape evolution with a migrating channel. (a) The channel boundary is represented explicitly by vectors. Arrow indicates general flow direction for all panels. (b) The plan view channel extent is recorded by mapping the bank locations onto a grid, which may represent topography or material composition and is altered during channel migration. Cells fully contained within the channel extent are shaded light gray. (c) When the channel banks shift (dashed lines), some cells are abandoned (medium gray) while other cells become enclosed by the channel (black). The process of updating the grid is spatially discontinuous, such that bank migration is not fully recorded with the grid.

grids are used in scenarios with only lateral differences bank-material properties [*Howard*, 1996; *Sun et al*., 1996, 2001; *Lancaster*, 1998; *Finnegan and Dietrich*, 2011] whereas three-dimensional grids are used to additionally track vertical variations in these properties [*Clevis et al*., 2006; *Karssenberg and Bridge*, 2008; *Sylvester et al*., 2011]. In some cases, the grid stores elevation or bank-material properties which alter the channel trajectory [*Howard*, 1996; *Sun et al*., 1996; *Lancaster*, 1998; *Güneralp and Rhoads*, 2011; *Motta et al*., 2012b], while in other cases, the grid is solely a framework for recording channel-influenced topography [*Finnegan and Dietrich*, 2011] or stratigraphy [*Clevis et al*., 2006; *Karssenberg and Bridge*, 2008; *Sylvester et al*., 2011]. Most commonly, active channel banks are represented using high-resolution vectors tracked independent of the grid (Figure 1a) [*Howard*, 1992, 1996; *Sun et al*., 1996; *Finnegan and Dietrich*, 2011], which we follow here. Grid-resolution dependencies come into play when areas previously occupied by the channel are recorded in the landscape by mapping the bank vectors onto a discrete grid of comparatively low resolution (Figure 1b). Consequently, as the banks smoothly migrate, some grid cells are abandoned while others are newly enclosed within the channel, but the process of updating the grid is discontinuous (Figure 1c). Therefore, past bank positions are incompletely recorded in the grid, and the maximum resolution for differentiating successive bank positions is the grid cell size.

[10] *Lancaster* [1998] adopted a distinct approach that recorded bank-material evolution using an adaptive irregular grid within the Channel-Hillslope Integrated Landscape Development model [*Tucker et al*., 2001]. In this framework, the channel centerline is explicitly tracked using nodes, but bank migration is incorporated by adding nodes in the point bar region and removing nodes in the cutbank region after the channel migrates more than a threshold distance. The finest horizontal resolution attainable by this scheme is the wetted channel width [*Lancaster*, 1998], and reducing the remeshing threshold can be computationally expensive [*Udaykumar et al*., 1999; *Clevis et al*., 2006; *Liu*, 2010]. Thus, as with fixed regular grids, bank positions are discontinuously recorded.

3.2. Demonstration of Resolution Dependence in Grid-Based Models

3.2.1. Meandering Model Implementation

[11] To illustrate spatial resolution controls on bank interactions in grid-based models, we use a bank-material tracking model similar to *Howard* [1996] and *Sun et al*. [1996, 2001], which is briefly reviewed here. In this implementation, a channel with a rectangular cross section scours the land surface to the bed elevation as it migrates laterally. The channel is forced to maintain a fixed width by balancing cutbank erosion with point bar deposition. As in *Howard* [1996], *Sun et al*. [1996, 2001], *Lancaster* [1998], and *Finnegan and Dietrich* [2011], fluxes of sediment are not tracked explicitly; thus, all eroded sediment is assumed to contribute to point bar deposition or leave the system. Bank migration rates are driven by local and upstream-weighted channel curvature [*Howard and Knutson*, 1984]. The channel centerline and banks are represented using discrete nodes connected by straight segments, a geometry common to many meandering models [*Crosato*, 2007]. The relative centerline migration rate (R_1) is calculated as

$$R_1(s) = \Omega R_o(s) + \frac{\Gamma \int_0^{\xi_{\max}} R_o(s-\xi)G(\xi)d\xi}{\int_0^{\xi_{\max}} G(\xi)d\xi} \quad (1)$$

where s is the node index, the dimensionless channel curvature is $R_o = (r/w)^{-1}$, r is the local centerline radius of curvature and w is channel width. The dimensionless weighting parameters Γ and Ω are set to 1 and -2.5, respectively, after *Ikeda et al*. [1981]. ξ is the upstream distance, and G is an exponential weighting function

$$G(\xi) = e^{-\left(\frac{2kC_f}{h}\right)\xi}. \quad (2)$$

Here k is a dimensionless scaling parameter equal to 1 [*Ikeda et al*., 1981], C_f is a friction coefficient (set as 0.01 after *Stølum* [1996]), and h is the channel depth. The curvature

integration proceeds upstream to the distance $\xi_{\max}$, where the normalized value of the weighting function G falls below 1%. The local lateral erosion rate ($E_L(s)$) is then computed for the sinuosity (μ) and the bank erodibility coefficient (k_e) as

$$E_L(s) = k_e R_1(s) \mu^{\varepsilon} \tag{3}$$

where $\varepsilon = -2/3$ [*Howard and Knutson*, 1984]. The bank erodibility coefficient k_e is set to yield the user-defined, space-averaged lateral migration rate.

[12] We track different classes of material in the river valley. For example, point bar sediments that are deposited along the inner bank by the river may have different strength properties than preexisting sediment or bedrock, sediment fill in abandoned cutoff loops, or floodplain deposits. In the course of each simulation, two-dimensional grids of land-surface topography and material properties are updated with the movement of the channel; thus, only lateral differences in bank-material properties are considered. A bank-material erodibility coefficient (k_e) is assigned to each intersected grid cell and is a linear function of the fraction of the bank comprised by each material of differing erodibility

$$k_e = \sum k_i f_i \tag{4a}$$

where f_i is the fraction of the bank (from the channel bed to the bank-full elevation) that has an erodibility k_i. For example, in the common case of differences in bank strength between bedrock and sediment, equation (4a) becomes

$$k_e = k_s(1 - f_b) + k_b f_b \tag{4b}$$

where f_b is the fraction of the bank (from the channel bed to the bank-full elevation) that is bedrock and k_s and k_b are the erodibilities of sediment and bedrock, respectively. The linear dependence of bank strength is similar to the parameterization of bank height influences on channel migration rates used by *Lancaster* [1998].

[13] The bank bedrock fraction is recalculated for each cell intersected by a test vector extended from the cutbank node in the direction of bank migration. The test vector length ($d_{\max}$) is calculated for each node as

$$d_{\max}(s) = k_{e,\max} R_1(s) \mu^{\varepsilon} \Delta t \tag{5}$$

where $k_{e,\max}$ is a fixed constant that represents the maximum erodibility amongst all bank materials present in the simulation, and Δt is the time step. This formulation ensures that the bank-material properties are inspected over a length scale long enough to account for the maximum possible bank migration distance but no further. The test vector length varies in response to the local relative migration rate at each node ($R_1(s)$) and so varies from node to node and through time. Thus, the length of the test vector is set before any information about the local bank composition has been ascertained.

[14] The erodibility can vary with distance from the channel banks in a given time step, so channel migration would proceed too far or not far enough if erodibility were only considered right at the banks. Therefore, to determine the appropriate bank migration distance, we define a "cost" for each increment of bank migration through material of constant erodibility. The cost represents the time required to migrate through that area relative to the time required to migrate through an area with the highest erodibility. For example, areas with relatively low erodibility take longer for the channel to migrate through and incur relatively high cost. The cost of bank migration through each cell intersected by the test vector is recorded and is equal to the ratio of the distance traveled within the cell (d_n) to the length of the test vector ($d_{\max}$), divided by of the erodibility for that grid cell ($k_{e,n}$). The channel bank node is moved incrementally until the cost function sums to 1, i.e.,

$$\sum_{n=1}^{N} \frac{d_n}{k_{e,n} d_{\max}} = 1 \tag{6}$$

where N is the number of cells traversed by the test vector. This formulation ensures that the actual bank migration distance properly accounts for the erodibility of all materials encountered in that time step. For example, the actual bank migration distance only equals the maximum possible bank migration distance ($d_{\max}$) when all of the material encountered by the search vector has the highest erodibility found in the model domain.

[15] The initial separation distance between channel centerline nodes (l) is equal to the channel width. In plan view, nodes move perpendicular to the channel centerline in the direction specified by the sign of $E_L(s)$ (positive to the left, looking downstream). Node-to-node distances along the centerline change as meander bends evolve; consequently, nodes are added and removed following rules similar to *Howard* [1984]. When two consecutive nodes (A and B) become separated by $2\,l$, an intervening node is added. When a node B is less than $0.5\,l$ from its upstream neighbor A but greater than $0.5\,l$ from its downstream neighbor C, B is shifted to a point equidistant from A and C. When any three consecutive nodes (A, B, and C) are oriented such that the distances from A to B and B to C are both less than $0.5\,l$, B is removed.

[16] New node locations are calculated using a local spline interpolation of the channel centerline. This local interpolation method bounds the node-to-node distances to the range $0.5\,l$ to $2\,l$, or $0.5w$ to $2w$ when $l = w$, where w represents the channel width. *Crosato* [2007] recommended $l > 0.3w$ to reduce numerical artifacts in centerline evolution, and $l < w$ to limit the visual effect of the centerline discretization. Maintaining the node spacing within this narrower range requires globally reinterpolating the channel centerline. While such an approach is desirable for constant bank strength cases such as those presented by *Crosato* [2007], our preliminary tests showed that reinterpolating the entire centerline in cases with variable bank strength suppresses channel migration in areas of slow channel migration. This occurs because reaches that migrate quickly through weak bank materials set the frequency of centerline interpolation. As a result, areas that migrate slowly through strong bank materials are reinterpolated too frequently, which locally straightens the centerline and inhibits meander bend growth. To our knowledge, this numerical artifact has not been identified in previous studies. Although the local interpolation approach adopted here places looser constraints on the centerline node-to-node distance than would a global interpolation approach, it allows for slowly migrating reaches to undergo centerline interpolation less frequently than quickly migrating reaches and thus does not inhibit meander bend growth.

[17] A periodic boundary condition is employed in three respects. First, the channel planform is periodic along the valley axis, such that meander bends that migrate across the downstream edge of the model domain reappear on the

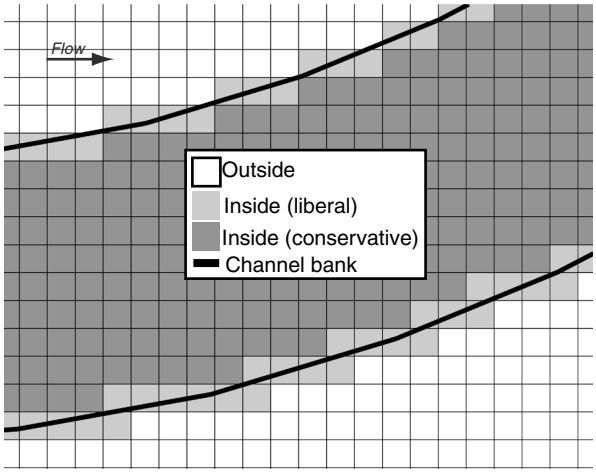

Figure 2. Comparison of rules for determining which grid cells are considered inside the channel banks, after *Howard* [1996]. Dark-shaded cells are completely within the channel, meeting the conservative in-channel definition. Light-shaded cells meet the conservative and liberal definitions, for which any cell partially traversed by the bank is also considered within the channel. Arrow indicates general flow direction.

upstream side, and vice versa. No channel centerline nodes are fixed, so the channel axis can drift freely. The extent of the model domain parallel to the valley axis scales with the average meander wavelength and is long enough that the channel curvature integration never spans the entire channel centerline. Second, the channel curvatures are computed in a periodic fashion, in accordance with the periodicity of the channel planform. Third, longitudinal profile elevations are periodic. Just as the channel centerline repeats with a lateral offset equal to the valley-parallel centerline distance range within the domain, the vertical component of the longitudinal profile repeats with a vertical offset equal to the vertical range of the long profile within the model domain. This ensures that reaches that enter the model domain on the upstream side are no lower than reaches downstream, and vice versa.

[18] Neck cutoffs occur whenever one of the channel banks intersects itself; chute cutoffs are not modeled. Because there is no subgrid parameterization for determining the bank position, a criterion must be established for whether or not a cell is considered within the channel. In this regard, *Howard* [1996] mentioned two end-member cases: (1) a conservative case, in which a cell must be fully contained by the banks to be considered within the channel and (2) a liberal case, in which any cell partially contained by the banks is also considered within the channel. Both cases are illustrated in Figure 2; the conservative case is adopted here to illustrate the resulting strong grid-resolution dependence of landscape evolution. The liberal case could also be adopted; it would consistently overpredict the area affected by channel migration because even partial bank migration across a cell boundary would result in alteration of bank-material properties for the entire cell.

3.2.2. Grid-Based Model Application and Results

[19] For the simulations presented in this subsection, we model the evolution of a river channel incising into bedrock and with mixed alluvial and bedrock banks that evolve in composition throughout the simulation. Specifically, the channel migrates 20 times faster in areas it has already visited (where it erodes through previously deposited sediment, i.e., $k_s = 1$) than it does when eroding against unvisited areas (which are entirely bedrock, i.e., $k_b = 0.05$). We track grids of land-surface topography and bedrock topography, the difference between the two being the sediment depth. Initially, the grid elevations are equal in elevation because the landscape is entirely bedrock. As the channel migrates laterally, the depth to bedrock is reset to the channel bed elevation. Cells abandoned by the channel are assigned a new elevation equal to the bedrock elevation plus the channel depth, which enacts sediment deposition along the trailing bank. The channel begins in a high-sinuosity state at the beginning of the simulations. The initial channel planform morphology is set by evolving the centerline in an identical simulation, except in the absence of bank-strength variations, from an initial straight centerline seeded with meter-scale noise. Channel bed elevation is set to be constant for simplicity and there is neither aggradation nor vertical incision.

[20] Three simulations were performed where the only difference between simulations was the grid resolution (Figure 3). A number of phenomena are common to all three simulations. The channel migrates, and the bank-material tracking grid records areas visited by the channel. Meander bends elongate, and several experience neck cutoffs. The bank material evolves in time as the channel erodes bedrock and deposits sediment, commonly on the inside of growing meander bends. The evolving bank materials also influence channel planform development: Straightened reaches form because bedrock banks slow bend growth in reaches that have experienced neck cutoffs. In places, the channels turn sharply where they transition from primarily sediment to primarily bedrock cutbank materials.

[21] Despite these similarities, the simulations also show that the small-scale representation of bank composition dramatically influences channel and bank-material evolution. The area visited by the channel (Figure 3a–3c) declines precipitously as the grid-cell width increases. As compared to the simulation shown in Figure 3a, which has a finer grid resolution, the simulation in Figure 3b shows slightly less area has been visited and also that the final channel position is different. In Figure 3c, the cell width is larger still; and though the cell width is less than the channel width, old meander loops are discontinuously recorded in the grid. Consequently, the visited area recorded in the grid is far less than in Figures 3a and 3b, and the final channel planform is again different from both cases. The pattern of grid cells crossed by the final channel extent (Figures 3d–3f) shows that finer grid resolutions result in more area recorded as visited by the channel.

[22] Despite starting with the same channel planform, the channel trajectory differs for all three simulations because the different grid resolutions cause different spatial distributions of bank strength to evolve. These differing bank-material properties cause reaches with similar geometries to migrate at different rates, which quickly causes the channel planform shapes to diverge. This implies that in general, model predictions for short-term channel trajectory and large-scale landscape evolution depend strongly on the grid resolution. Depending on the model outcome considered, the resolution artifact may greatly distort the influence of bank-material properties.

[23] One solution to remove the dependency of landscape evolution on grid resolution is to decrease the grid cell size

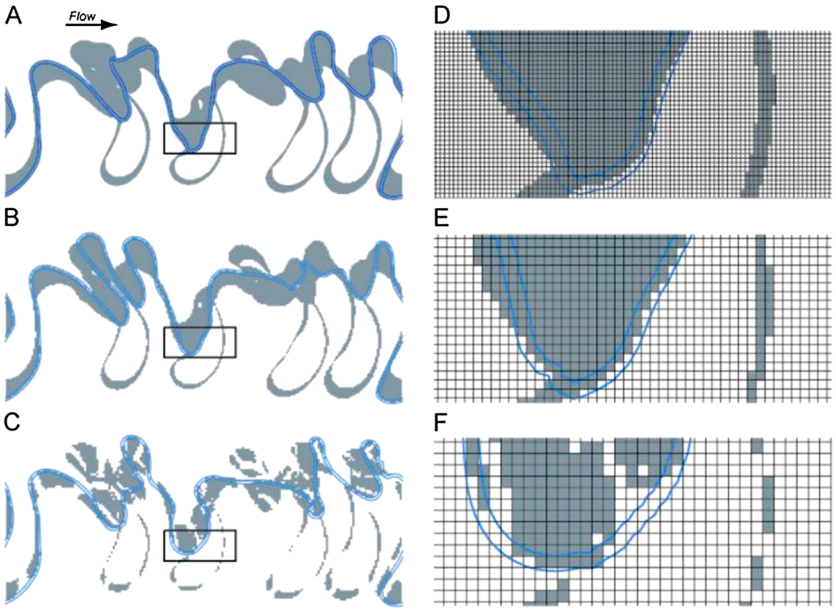

Figure 3. Simulations of a meandering river using grid-based bank-material tracking. Channel banks are indicated in blue; areas that have been visited by the channel, as recorded by the grid, are mantled with sediment and shaded gray. Bedrock is 20 times more resistant to erosion than sediment. (a–c) Final simulation conditions are shown, with boxes indicating the extents of (d–f) detailed views. Arrow in Figure 3a indicates general flow direction for all panels. Topography and bank composition are recorded using rectangular grids with cell widths of 7 m in Figure 3a, 14 m in Figure 3b, and 18 m in Figure 3c. Channel width is 25 m. The area visited by the channel changes dramatically as a function of grid resolution, with all other parameters held constant. Figures 3d–3f show the detailed relationship between the final channel bank vectors and the grids.

so that it is much smaller than any incremental change in the river channel location. To illustrate this point, the cell width (Δx) can be nondimensionalized ($\Delta x'$) using the migration length scale

$$\Delta x' = \frac{\Delta x}{E_L \Delta t} \tag{7}$$

where E_L is the mean lateral erosion rate; a solution that is independent of grid resolution would require $\Delta x' \leq 1$. In practice, however, such a resolution is difficult to achieve given memory constraints, especially for model cases run over geomorphic timescales where E_L and Δt are small. As an example, bankfull river floods often occur at approximately annual timescales ($\Delta t = 1$ yr) and bedrock erosion rates are typically on the order of $E_L = 1$ mm/yr, which implies a minimum memory footprint of 1 TB per square kilometer of model domain using a uniformly spaced rectangular grid, a memory requirement that can only be met by supercomputers. Due to these memory limitations, coarser grid resolutions are exclusively used in practice. For example, the cell width in the *Howard* [1992, 1996] and *Sun et al.* [1996, 2001] models and the threshold distance for node addition in *Lancaster* [1998] are approximately one channel width. Alluvial meandering rivers typically migrate at less than one tenth of a channel width per year [e.g., *Nanson and Hickin*, 1983; *Hudson and Kesel*, 2000]. Taking this as an upper bound for the bank migration rates and assuming an annual time step yields approximate values of $\Delta x' = 10$ (for extremely rapid migration at 0.10 widths per year) to 100 (for a more typical migration rate of 0.01 widths per year) for the aforementioned studies.

[24] Because lateral erosion rates vary spatially for meandering channels [*Nanson and Hickin*, 1983; *Hudson and Kesel*, 2000], bends that migrate relatively slowly may be affected by grid resolution even if other bends are not. Consequently, existing frameworks for landscape evolution in meandering environments with bank strength differences generally yield grid-resolution dependent results except for cases with very large lateral migration rates. The grid resolution issue is especially significant for rivers with bedrock banks, which have lateral migration rates of millimeters to centimeters per year even in relatively weak rock [*Hancock and Anderson*, 2002; *Montgomery*, 2004; *Fuller et al.*, 2009; *Finnegan and Dietrich*, 2011].

4. A New Vector-Based Method for Modeling Meandering-Landscape Interactions

[25] In light of the resolution dependence of bank-material properties and channel trajectories in grid-based approaches to modeling meandering-landscape interactions, we propose a new framework for tracking bank-material geometry. The framework builds off the stratigraphic visualization approaches of *Pyrcz and Deutsch* [2005] and *Pyrcz et al.* [2009], which use a channel's extent and longitudinal profile as reference objects for identifying simultaneously formed fluvial deposits. In these studies, modeled stratigraphy is formed by assembling channel extents from different points in its trajectory. We extend this

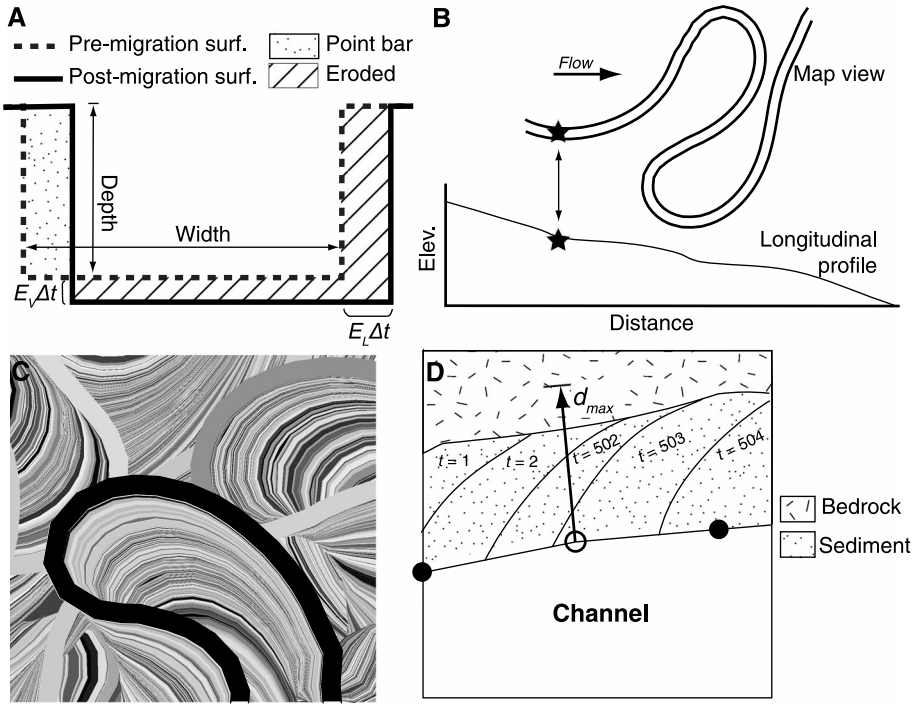

Figure 4. The new, vector-based method for erodibility and topography tracking. (a) Lateral channel migration and vertical incision of a rectangular channel during one time step is viewed in cross section. Dashed line indicates the premigration surface. During each time step, the channel cross section is shifted laterally and vertically to form the postmigration surface (thick black line) and erode material from the bed and cutbank (hatched area). In order to maintain constant channel width, point bar sediment (dotted area) is deposited over the abandoned surface with a thickness equal to the channel depth. (b) The channel map view extent and longitudinal profile from each time step are used to reconstruct bank-material properties. (c) After subsequent iterations, the pattern of channel scour is recorded by the current channel extent (black polygon) and the collection of abandoned channel-extent polygon remnants preserved from earlier in the simulation, with channel extents shaded to highlight their different formation times. (d) Map view of the bank-material inspection procedure. A meandering model is used to calculate the maximum centerline migration distance ($d_{\max}$) assuming the most erodible bank material. A test vector with length equal to $d_{\max}$ is extended perpendicular to the cutbank node and is used to identify regions with different bank-material properties and adjust the actual migration distance accordingly. In this example, the test vector encounters sediment-mantled surfaces from different time steps ($t = 503$, 502, and 2, in order) followed by a bedrock valley wall.

approach by including interactions between the channel trajectory and the properties of the bank material. In contrast to the method of recording bank-material properties with grids, in our new approach, topography and bank-material properties are recorded using initial valley geometry and the full history of channel positions, which are stored as vector data. As the channel migrates and encounters areas it has previously visited, the new algorithm queries a database of previous channel positions to reconstruct these bank-material properties instead of querying a bank-material grid. The database of channel positions is used to define polygonal regions of bank material formed during the simulation where the node spacing along the polygon boundaries is set by the channel boundaries themselves. Therefore, there is no data degradation with respect to the geometry produced by the underlying meandering model, as occurs in mapping the channel boundaries onto a grid.

[26] To illustrate the new vector-based approach for tracking bank-material properties, we use the same model to drive channel migration [*Howard and Knutson*, 1984] as in section 3.2.1. At each time step, the channel translates laterally by the local lateral erosion rate times the time step ($E_L\Delta t$) and vertically by vertical erosion or aggradation rate times the time step ($E_V\Delta t$) (Figure 4a). The channel is forced to maintain a constant width, and point bar sediment (with thickness $\Delta z_{\text{point bar}}$) is assumed to accumulate on the trailing bank to the height of the flow depth. To calculate the vertical erosion or aggradation rate, an evolution equation such as the stream power equation [*Howard and Kerby*, 1983] can be applied to the longitudinal profile. To introduce the bank interaction algorithm, we discuss a case with only lateral differences in bank-material properties. The general principles used for bank-material tracking also extend to cases with vertically stratified bank materials, however, and we present one such example in section 5.3.

[27] The bank interaction algorithm proceeds as follows. A meandering model is used to compute a preliminary, bank strength-independent lateral migration rate for each centerline node. The channel banks are tracked as separate vectors, and each left and right bank node is associated with a centerline node. The local channel migration direction determines which bank node represents the trailing bank and which represents

the cutbank. At each time step, the bank vectors are used to construct the planform extent of the channel. The local elevation of the channel bed within this extent is calculated by interpolating along the channel longitudinal profile (Figure 4b) and can be refined using vector-based cross-section data that is also stored. The channel bed elevation represents the elevation to which the channel bed scoured the land surface (z_{scour}) at the time the channel extent occupied that location. Thus, whereas the grid-based method would look up z_{scour} from a grid of elevation values that spans the model domain, the vector-based method determines z_{scour} using only the past positions of the channel. The channel planform extents from different time steps collectively characterize the areas of a valley scoured by channel migration (Figure 4c).

[28] Because channel geometric information is saved at every time step, reconstructing bank-material properties becomes more computationally intensive as the simulation proceeds. Part of this operation is to determine which of the saved previous channel locations are needed to reconstruct the local elevation and composition of bank material. Rather than search the entire channel geometry database, we use an indexing system that associates each channel extent with an approximate time interval and spatial location. We query this database to find the most recent time of channel occupation in order to determine local bank-material properties. The most recent time is used because when the channel migrates across an area, it updates the landscape properties set during earlier instances of channel occupation. The spatial and temporal indexing increments are user defined, can vary during the simulation, and do not affect the model results; they only affect the efficiency of the bank-material look-up operations.

[29] To account for variable strength material in the calculation of local lateral migration distance, we use the test vector approach as described in section 3.2.1 (equation (5); Figure 4d). Bank-material properties are reconstructed at points along this test vector separated by an interval distance of $E_L\Delta t$. Parts of the model domain beyond the channel-visited area are represented by a valley-bounding polygon which is user defined and can represent an arbitrary topography and bank-material composition. In the example in Figure 4d, the test vector encounters sediment and bedrock, and therefore, the local migration distance is adjusted according to these different erodibilities (equation (6)).

[30] Once the original channel scour depth is determined, it is used to calculate the land surface elevation (z)

$$z = z_{\text{scour}} + \Delta z_{\text{point bar}} + \Delta z_{\text{overbank}} \tag{8}$$

where $\Delta z_{\text{point bar}}$ represents the thickness of point bar deposits and $\Delta z_{\text{overbank}}$ is the elevation contribution from overbank deposition. The locations of meander cutoff loops are tracked independently so that areas abandoned by the channel through cutoffs are not assigned a mantle of point bar deposits. Equation (8) applies only outside of the channel; within the channel, the elevation is equal to z_{scour}. Overbank deposition can be incorporated using different models. Here we choose the model of *Howard* [1996]

$$\frac{dz_{\text{overbank}}}{dt} = \eta + D_s e^{-d_c/\lambda} \tag{9}$$

where dz_{overbank}/dt is the rate of elevation change within the floodplain; η is a constant deposition term; and the second term is a spatially dependent overbank deposition rate, where D_s is the deposition rate of overbank sediment at the channel banks, d_c is the minimum distance to the active channel, and λ is a decay length scale. Within the vector-based framework, the local sediment cover due to overbank deposition is determined by calculating the overbank sediment contribution from the channel at each time step after the channel abandoned the point

$$\Delta z_{\text{overbank}} = \sum_{t=t_a+\Delta t}^{t_f} \left(\eta + D_s e^{-d_c(t)/\lambda}\right) \tag{10}$$

where t is time, t_f is the current model time, t_a is the time the channel abandoned the point, and $d_c(t)$ is the minimum distance from the point to the channel at time t. A gridding procedure, used to visualize the final topography, can be performed at arbitrary resolution. This is because the elevation at any particular point is not stored explicitly but rather is calculated as needed to determine bank-material height. To do this, the algorithm uses the channel polygon that contains the point of interest, retrieves the time step associated with the channel polygon from the database of previous channel positions, and projects the point onto the longitudinal profile associated with that time step to reconstruct the original channel scour depth. Adding contributions from point bar and overbank sedimentation yields the exact elevation.

[31] The channel scour and land surface elevations are bank-material properties that can be used to define an effective bank erodibility, which is a user-defined function (e.g., of bank elevation and composition) and can vary with the application as in section 3.2.1 (equation (4a)). A unique erodibility value is calculated for each interval between checkpoints along the test vector. The final lateral migration distance for each centerline node is calculated using the erodibility in each interval until the cost condition (equation (6)) is met. Once the final migration distance is calculated for each centerline node, the nodes are moved perpendicular to the local centerline azimuth by this distance, and the bank nodes track along with them.

[32] The memory required by the vector-based approach depends on the channel trajectory, which determines the size of the channel geometry indexing data structure. In trial simulations of bedrock river valley evolution, we noted a memory savings of at least 2 orders of magnitude over a grid-based model of equivalent resolution, because in the vector-based approach, areas with similar bank-material properties can be stored using their boundary coordinates instead of a grid of contiguous pixels. This is analogous to the efficiency offered by boundary element models as compared to finite element models used widely in engineering [*Katsikadelis*, 2002; *Li and Liu*, 2002; *Liu*, 2010].

5. Case Studies

[33] The vector-based framework for bank-material tracking can be applied to a broad array of systems with interactions between channels and bank material. In this section, we focus on four particularly common and diverse scenarios for rivers. First, we model floodplain evolution for a scenario in which a channel bed neither aggrades nor degrades, and material that accumulates in oxbows (abandoned meander cutoffs) has a different strength than point bar

sediments that accumulate by channel lateral migration. Second, we extend the floodplain development scenario to a case with channel aggradation and floodplain deposition to analyze the resulting stratigraphy. Third, we model topographic evolution by a meandering river incising a bedrock valley with mixed alluvial and bedrock banks that evolve in the simulation. Fourth, we model a case of overbank deposition by an alluvial river in which bank height rather than bank material determines erodibility. We begin by discussing aspects of the initial conditions and the model domain common to all four case studies.

[34] Grid- and vector-based tests within each case study use the same initial conditions, and the underlying meandering model is identical to that described in section 3.2.1. The channel bed is initially inset by one channel depth into a planar landscape with constant slope. The initial channel centerline is straight, with random perturbations of order 0.01 channel widths to seed meander development. The initial channel slope matches the landscape slope.

5.1. Bank Strength Effects on Floodplain Evolution

[35] The tendency for meandering channels to confine themselves within a narrow channel belt is a subject of ongoing debate. Cutoffs inherently limit channel sinuosity and meander-belt width [*Howard*, 1996; *Camporeale et al*., 2005], but fine-grained, oxbow-filling sediments have been argued to further enhance meander-belt confinement because they tend to be more resistant to erosion than other floodplain materials [*Fisk*, 1947; *Allen*, 1982; *Ikeda*, 1989]. For example, *Hudson and Kesel* [2000] argued that fine-grained sediments in oxbows account for large spatial variability in bank migration rates along the Mississippi River, U.S. This mechanism implies a feedback between meander growth, cutoff, and overbank sedimentation and was simulated in *Howard* [1996] and *Sun et al*. [1996]. Both studies suggested that oxbow sediments could steer the trajectory of subsequent meanders and potentially facilitate self confinement of meander belts. However, given the relatively coarse grids used in these studies, the grid resolution itself could have caused greater meander belt confinement. Thus, determining the relative importance of these confinement mechanisms requires accurate modeling of bank-material properties.

[36] The vector-based framework presented here can contribute to a better understanding of the temporal and spatial scales associated with the coevolution of meandering rivers and floodplain material properties and can quantify grid-resolution effects inherent in the models of *Howard* [1996] and *Sun et al*. [1996]. To demonstrate this, we reproduce the style of clay plug resistance modeled by *Howard* [1996]: Abandoned meander loops are set to instantly fill with sediment more resistant than the rest of the floodplain, and the overbank sedimentation outside of oxbows is set to zero. The relative erodibility of cutoff fill compared to point bar sediment (k_{ec}) is varied between 0.01 and 1, spanning a range explored in *Howard* [1996] and *Sun et al*. [1996]. The portions of cutoff loops within three channel widths of the closest channel bank at the time step following cutoff are set to infill with material equivalent in erodibility to point bar sediments [*Howard*, 1996]. *Sun et al*. [1996] additionally modeled cases with time-dependent bank-material strength due to progressive infilling of oxbows with relatively resistant sediments. Though not implemented for this case study, such scenarios could similarly be modeled using vector-based bank-material tracking because surface or deposit age is saved along with bank-material polygon geometry.

[37] Figure 5 compares the resulting topography for simulations using grid-based and vector-based bank-material tracking. In Figures 5a–5c, $k_{ec} = 1$, so there are no bank strength contrasts. Consequently, these three panels show identical final planform geometries because only bank strength differences that arise during these simulations can cause the geometries to diverge. Except for the coarse grid case (Figure 5a), all simulations show an active record of meander bend growth and cutoff and that the channel axis drifts. Abandoned meander cutoffs are numerous and distributed across the area and commonly intersect one another, similar to Johnson Creek, Yukon Territory, Canada [*Camporeale et al*., 2005], for example. In cases with resistant oxbow-filling sediments ($k_{ec} = 0.1$; Figures 5d–5e), the portion of the meander belt that was recently visited by the channel is confined to the center of the valley where oxbow remnants are relatively rare. In the cases with no bank strength differences ($k_{ec} = 1$; Figures 5b–5c), the recently visited area tends to the top half of the model domain, and the numerous oxbows in this area have no influence on the channel migration.

[38] When the grid resolution is relatively coarse and equal to the channel width (Figure 5a), little of the channel migration is recorded in the topography because it is rare for the channel banks to instantaneously enclose full cells. With a finer grid resolution of $0.4w$ (Figure 5b), where w is the channel width, the visited area more closely resembles that for the vector-based case (Figure 5c), and the final channel planform extents coincide. Cutoff loops are thinner in the grid-based cases (Figures 5b and 5d) than in the vector-based cases (Figures 5c and 5e) because the channel width spans some cells incompletely in the grid-based case, and the bank-material in these cells is not recorded as cutoff loop-filling sediments. The floodplains are expected to be the same in these two cases because the channel migration does not interact with evolving bank-material properties.

[39] Topography differs in subtle but potentially important ways between the fine grid- and vector-based simulations when $k_{ec} = 0.1$ (Figures 5d–5e) and spatially variable bank materials are allowed to evolve. Most importantly, despite beginning with the same channel planform extent, the two cases differ in the final channel planform extent and the geometry of the active meander belt. This occurs because the finite resolution at which the grid-based case stores bank-material composition leads to divergent bank-material properties and channel trajectories.

[40] Calculation of the mean active width of the meander belts in these simulations allows for more quantitative comparisons (Figure 5f). We define the mean active meander-belt width as the area modified by the channel in the last 10% of simulation time divided by the left-to-right length of the model domain. The coarse grid resolution simulations ($\Delta x = w$) record only fragments of the channel migration regardless of the relative erodibility of oxbow sediments, which results in a minimal active meander belt width. When the grid resolution is higher ($\Delta x = 0.4w$), the mean active width increases as a function of k_{ec}. The vector-based approach shows the same relationship, and the grid-based and vector-based approaches give equivalent results when $k_{ec} = 1$ because bank strength is uniform. When $k_{ec} < 1$, the vector-based method yields a larger mean active meander-belt width than the grid-based case ($\Delta x = 0.4\ w$), and this discrepancy increases as the erodibility

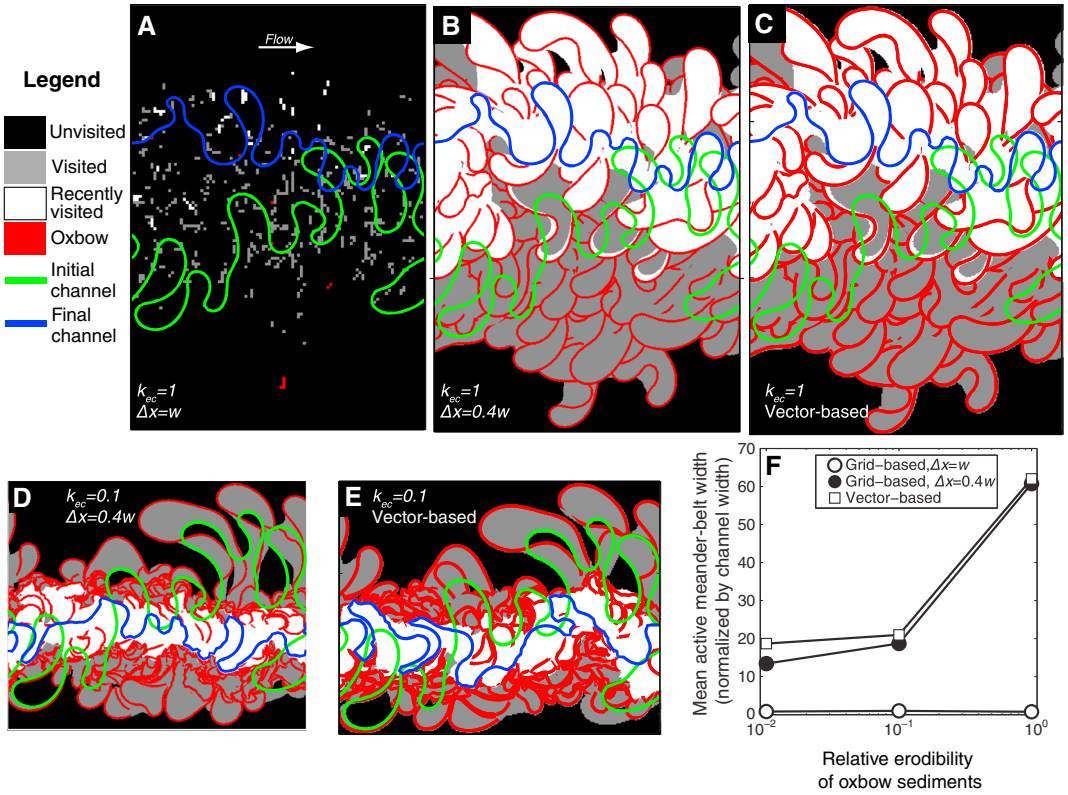

Figure 5. Meander-belt evolution with variable erosion susceptibility for meander cutoff loops (k_{ec}) relative to point bar sediment. The left-to-right width of all map-view panels is 100w. In all simulations, $\Delta t = 2$ yr, simulation time is 1000 yr, $w = 25$ m, and $h = 1$ m. Areas recorded as visited by the channel are shaded gray (first 90% of simulation time) and white for recently visited areas (last 10% of simulation time). Unvisited areas, as recorded in the grid- or vector-based tracking schemes, are black. Initial (green) and final (blue) channel extents are indicated, as are remnants of oxbow sediments (red). Figures 5a–5c represent the case of $k_{ec} = 1$, i.e., constant bank composition. Figure 5a shows that a coarse grid resolution ($\Delta x = w$) results in a small area recorded as visited. Arrow indicates general flow direction for all panels. With a finer grid resolution ($\Delta x = 0.4w$) (Figure 5b), the visited area more closely resembles that using vector-based tracking (Figure 5c). Figures 5d–5e represent $k_{ec} = 0.1$, i.e., erosion-resistant material is stored in cutoff loops. Figure 5d shows the grid-based case, with $\Delta x = 0.4w$. Figure 5e shows the vector-based case. (f) Mean active meander-belt width (normalized by channel width, w), versus the relative erodibility of oxbow sediments (k_{ec}) for grid- and vector-based schemes.

contrast between oxbow and other sediments increases. The meander belt in the grid-based case is about 40% narrower than for the vector-based case when $k_{ec} = 0.01$. Mean active meander-belt width decreases with decreasing k_{ec} because the channel migrates more slowly through oxbow sediments and thus becomes confined to a narrower area. The vector-based case shows less narrowing than the grid-based case ($\Delta x = 0.4w$), however, because in the grid-based case the channel must sweep entirely across a cell in order to reset its bank strength. This makes channel-confining oxbow sediments more persistent than in the vector-based case, for which there is no such threshold for updating bank strength. As a result, the channel can reset bank strength more easily in the vector-based case and can maintain a wider mean active meander-belt width.

[41] Vector-based simulation results demonstrate that oxbow sediments that are less erodible than other floodplain sediments can indeed confine the active width of meandering. Thus, while cutoffs play a role in confining the meander belt [*Camporeale et al.*, 2005], bank strength differences established by channel migration should result in narrower meander belts than would be predicted based on cutoff-driven confinement alone (i.e., when $k_{ec} = 1$). A significant proportion of the meander-belt narrowing predicted using grid-based models is due, however, to a numerical artifact.

5.2. Bank Strength Effects on Channel Body Geometry

[42] Meander-belt evolution in aggrading rivers is a prime determinant of the stratigraphic architecture of the resulting fluvial deposits, with important implications for reservoir analysis including the connectivity of porous and permeable sand bodies [*Henriquez et al.*, 1990; *Hirst et al.*, 1993]. To illustrate the potential for differential bank strength to influence deposit geometry, we model a scenario equivalent to the floodplain evolution case in section 5.2, but here we force the river to aggrade at a constant rate. *Sylvester et al.* [2011] presented a similar model scenario but without variable bank strength. As in the previous case study, oxbows are set to instantly fill with sediment whose erodibility is a fraction (k_{ec}) of the erodibility of point bar sediment. Outside of oxbows, overbank sediments must accumulate

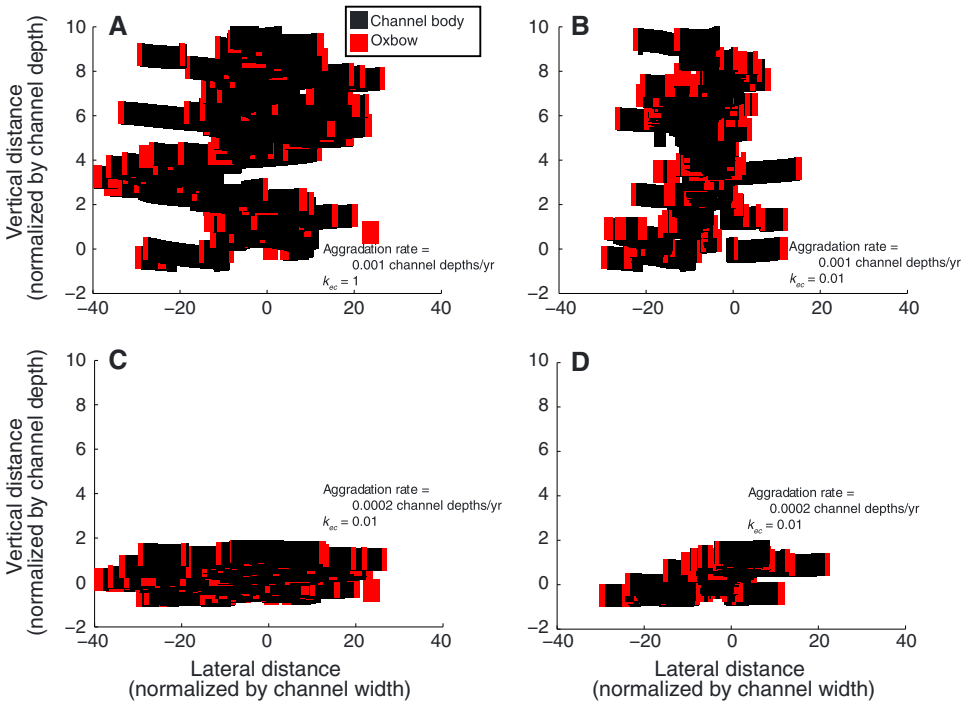

Figure 6. Cross-valley cross sections of stratigraphy formed by an aggrading, meandering channel. As the channel migrates, it deposits channel body material (black) and distinct sediments in oxbows (red). Other overbank deposits, not shown, accumulate at a rate sufficient for the channel to remain confined and have a material strength equal to that of channel body material. For all simulations, $w = 25$ m; $h = 1$; the maximum lateral migration rate is 1 m/yr for erosion of channel body deposits; $\Delta t = 2$ yr; and simulation time is 10 kyr. Vertical axes are scaled to channel depth and horizontal axes are scaled to channel width. k_{ec} is the relative erodibility of oxbow sediments. (a) Fast aggradation (0.001 channel depths/yr), $k_{ec} = 1$. (b) Fast aggradation, $k_{ec} = 0.01$. (c) Slow aggradation (0.0002 channel depths/yr), $k_{ec} = 1$. (d) Slow aggradation, $k_{ec} = 0.01$.

in order to maintain channel confinement. For consistency with *Howard* [1996] and *Sun et al*. [1996], which for the relevant simulations did not track overbank sediments that accumulated outside of oxbows, such overbank sediments are assumed to have no effect on bank strength (i.e., only fine sediments that accumulate in oxbows alter bank strength). While this is a highly idealized model for floodplain sedimentation, it allows isolating the kinematic role of oxbow-filling sediments in aggrading environments. We extend the two-dimensional approach to bank-material tracking used in previous examples to three dimensions by tracking the lateral and vertical extent of resistant sediments, in order to account for multiple layers of channel deposits.

[43] We compare cross sections perpendicular to the valley axis for scenarios with and without bank strength contrasts, for two different aggradation rates; all cases utilize vector-based bank-material tracking (Figure 6). For both high (0.001 channel depths/yr) and low (0.0002 channel depths/yr) channel aggradation rates, the total deposit width is approximately 50% larger in cases with no bank strength contrast ($k_{ec} = 1$; Figures 6a and 6c) than for cases with a bank strength contrast ($k_{ec} = 0.01$; Figure 6b and 6d). While under rapid aggradation with no bank strength contrast, channel bodies record channel axis drift (Figure 6a), which leads to spatial clustering of channel bodies similar to that commonly observed at larger scale in alluvial basins [e.g., *Hajek et al*., 2010]. The case with aggradation and a strong bank strength contrast results in a deposit with more tightly constrained lateral excursions (Figure 6b). This occurs because when deposits that accumulate in oxbows have a low relative erodibility, they impede channel lateral migration and hence overall deposit width. Taken together, these simulations indicate that vector-based bank-material tracking may be useful for constructing reservoir models when there are bank strength differences between sedimentary units, e.g., due to grain size differences [e.g., *Sylvester et al*., 2011].

5.3. Bedrock Valley Widening

[44] Bank strength in upland rivers varies strongly between sediment and bedrock, and in these environments, the vector-based method is well suited to represent the relatively slow erosion rates in bedrock. Extensive research has focused on quantifying rates and controls on river vertical incision in bedrock [see *Whipple* 2004, and references therein] and more recently bedrock channel width [*Finnegan et al*., 2005; *Wobus et al*., 2006; *Turowski et al*., 2008; *Yanites and Tucker*, 2010]. Processes that cause channel widening also contribute to bedrock valley widening and thus are important for understanding the large-scale evolution of mountain landscapes [*Montgomery*, 2004; *Whipple*, 2004]. To compare grid- and vector-based frameworks for recording bank-material composition for channels with mixed bedrock and alluvial banks, we construct a numerical experiment in which a channel migrates laterally and erodes vertically within an established valley. Similar to *Howard* [1996], the bedrock valley walls

are prescribed higher bank strength than bank material within the valley. Here we model a 100-fold bank strength contrast between bedrock and sediment, as is likely common in bedrock-walled valleys where valley widening rates of 1 cm/yr or less predominate [*Montgomery*, 2004].

[45] The longitudinal profile node farthest downstream in the model domain is lowered at a constant rate to drive relative base-level fall and vertical incision. The vertical erosion rate (E_V) is set to be proportional to the local bed shear stress [*Howard and Kerby*, 1983]

$$E_V = k_v \rho g h S. \tag{11}$$

The rate constant k_V is set to 0.003 to achieve an average incision rate of 1 mm/yr; ρ is the density of water; g is gravitational acceleration; h is the channel depth; and S is the local bed slope, calculated as a first order, forward finite difference. In order for a channel reach to remain confined during downstream translation, its rate of vertical incision must match or exceed the rate of elevation loss due to translation if the landscape slopes downstream, i.e., $E_V \geq E_L S_s$, where S_s is the mean slope of the surface over which the node migrates. Consequently, we limit our analysis to a case where $E_V \geq E_L S_s$ to avoid cases where the channel loses confinement through lateral migration on a tilted landscape.

[46] We model the evolution of the valley-bound channel using both grid-based and vector-based approaches to bank-material tracking for comparison. In both cases, the channel bends grow from an initial state of low sinuosity. Before bends can become highly sinuous and reach neck cutoff, however, the valley walls inhibit their motion. This results in angular channel planform extents where the channel deforms against the valley walls (Figure 7), similar to the Beaver River, Alberta, Canada [*Parker et al*., 1983; *Nicoll and Hickin*, 2010], for example. Because the bank material in valleys has lower strength than at the valley walls, meander bends preferentially drift down valley rather than across valley. This causes frequent planation of the entire valley floor, which lowers the sediment-bedrock interface and permits the channel to remain mobile and unentrenched within the valley. At the valley margins where there is a large contrast in bank strength between sediment and bedrock, the grid- and vector-based bank-material tracking schemes yield divergent behaviors.

[47] When bank material is modeled with a grid of 2 m ($0.08w$) resolution (Figure 7a), the channel is fully restricted to the initial valley width, and meander bends only propagate down valley. This occurs because the channel must advance a full cell width beyond the initial valley wall before updating the bank-material grid. Any bank advance less than a cell width is not recorded so that these minor advances leave no record of erosion and subsequent channel migration always encounters a fully intact valley wall unless the bank cumulatively advances through an entire cell.

[48] With the vector-based approach, the valley more than doubles in width as compared to the grid-based approach (Figures 7b and 7c). Lateral erosion, which is suppressed by the implicit erosion threshold in the grid-based case, occurs steadily in the vector-based case. The channel widens both sides of the valley but erodes more material from the top side of the model domain because channel axis drift—an inherent behavior in the underlying meandering model—can cause asymmetric erosion patterns.

[49] Vector-based bank-material tracking represents the kinematics of channel migration in environments with large bank strength contrasts without imparting inadvertent lateral erosion thresholds. This opens a number of opportunities for understanding the evolution of bedrock landscapes. Vector-based material tracking could enable the incorporation of physical models of channel width and meandering dynamics into larger-scale landscape evolution models. Consequently, the long-term behavior of different channel evolution models could be directly evaluated without the confounding effects introduced by grid-based bank-material representation. At a larger scale, the influence of channel migration on bedrock valley width and the formation of strath terraces [e.g., *Finnegan and Dietrich*, 2011] can be more accurately ascertained with vector-based bank-material tracking. Finally, links between external drivers—including climate, tectonics, and base level—and large-scale channel characteristics such as sinuosity [*Stark et al*., 2010] and entrenchment [*Harden*, 1990] can be more rigorously evaluated.

5.4. Floodplain Evolution With a Bank Height-Dependent Channel Lateral Migration Rate

[50] In the preceding case studies, erodibility differences result from differences in bank material composition. Here we assess a scenario in which bank materials are uniform, but bank height sets the local erodibility [e.g., *Lancaster*, 1998; *Parker et al*., 2011]. Figure 8 shows topography formed by a channel that migrates laterally and deposits overbank sediment over 1000 years, with a maximum lateral erosion rate of 1 m/yr, a constant deposition rate (η) of 10 mm/yr, and a spatially varying deposition rate of 3 mm/yr at the channel bank (D_s) with a decay length scale (λ) equal to four channel widths. For simplicity, meander cutoff loops are assumed to instantaneously fill completely with sediment. We consider a case in which lateral channel migration is independent of bank height (Figure 8a) and, similar to *Lancaster* [1998], a case in which lateral channel migration rates vary inversely with bank height scaled to channel depth (Figure 8b) as

$$E_L = E_L \left(\frac{z - z_{\text{channel}}}{h} \right)^{-1} \tag{12}$$

where z_{channel} is the local elevation of the channel bed. Equation (12) is applied so that bank height can only reduce lateral erosion rate (i.e., cases with $(z - z_{\text{channel}})/h < 1$ do not cause lateral erosion rate to increase). The channel bed is set to aggrade at a constant rate equivalent to the aggradation rate at a distance of four channel widths from the channel (i.e., the e-folding distance for distance-dependent overbank deposition) (equation (9)). Consequently, the levee tops aggrade faster than the channel bed. Levee growth is paced by the competition between overbank deposition that builds the levees and lateral channel migration that causes the channel to erode existing levees and shift the locus of deposition. This causes spatial differences in bank height that modulate channel lateral migration rates.

[51] Both cases show a highly sinuous channel that has undergone meander bend growth and cutoff, and cutoff loops are preserved in the floodplain topography, similar for example to the Sacramento River, California, U.S. [*Constantine and Dunne*, 2008]. Although both cases start

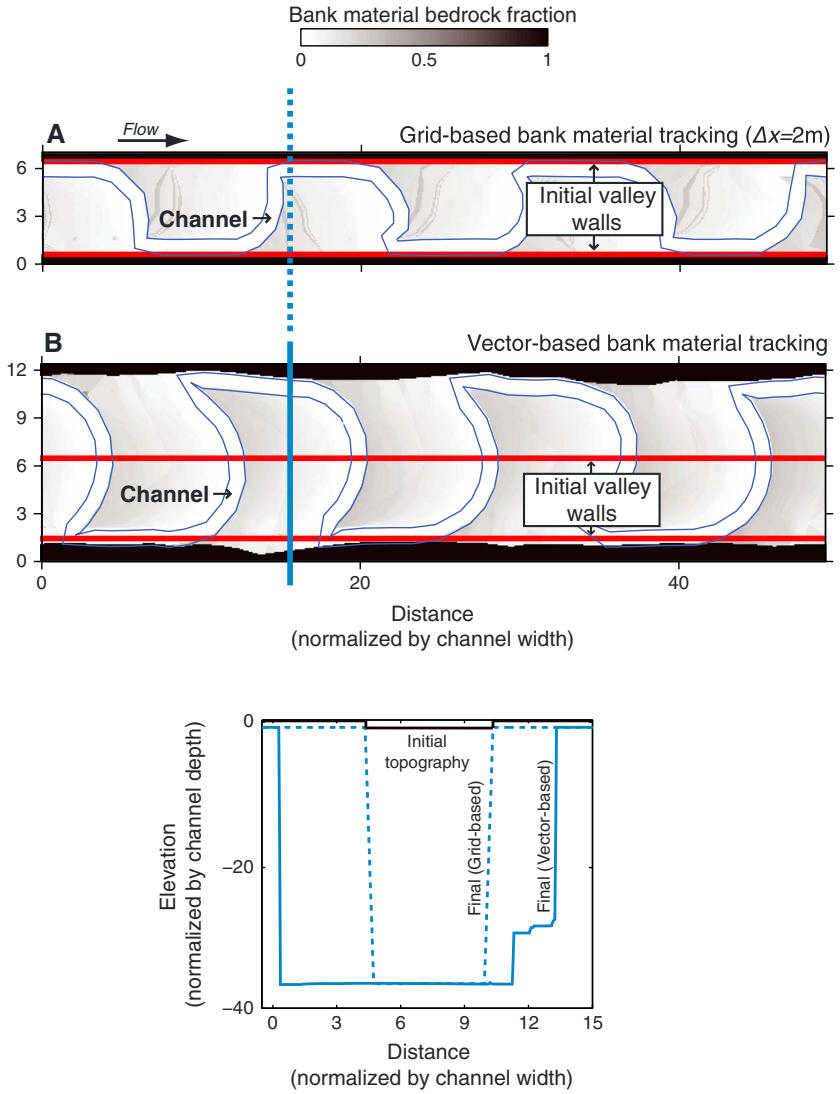

Figure 7. Valley widening in a bedrock landscape using grid-based and vector-based bank-material tracking. (a and b) Active channel banks are shown with thin blue lines. In both cases, $\Delta t = 2$ yr, simulation time is 40 kyr, the maximum lateral erosion rate in bedrock is 1 cm/yr, the maximum lateral erosion rate in sediment is 1 m/yr, $E_v = 1$ mm/yr at the outlet, $w = 25$ m, $h = 1$ m, and the initial valley width is approximately $5w$. Initially, the bank material within the valley floor is entirely sediment above the local elevation of the channel bed, and entirely bedrock below this elevation, such that the channel banks are all sediment. The channel bed begins entrenched one channel depth below the land surface. The valley walls are composed entirely of bedrock and initially have the same surface elevation as the valley floor. The fraction of bedrock in bank material, as sensed locally by the channel, is calculated by comparing the bedrock elevation to the bed elevation of the nearest point on the channel. Distance is normalized by the channel width and elevation by the channel depth. Figure 7a shows the simulated landscape using grid-based bank composition tracking, with $\Delta x = 2$ m, and there is no valley widening. Arrow indicates general flow direction for both panels. Figure 7b shows the simulated topography using the vector-based approach. Valley width more than doubles during the simulation because all bank advances beyond the initial valley wall extent are recorded. (c) Cross sections of the initial topography of both simulations (black line) and the final topography for the grid-based (dashed blue line) and vector-based (solid blue line) simulations.

with the same planform channel geometry, the modulation of lateral channel migration rate by bank height in Figure 8b causes the channel trajectories to diverge. Because topographic evolution is governed by channel scour and overbank deposition, these different channel lateral migration patterns result in differing topography. In both cases, topographic profiles (Figure 8c) show higher elevations near the active channel and abandoned channel segments in cutoff loops because overbank sedimentation declines with distance from the channel (equation (9)).

[52] These simulations demonstrate that while the vector-based method emphasizes tracking the planform extent

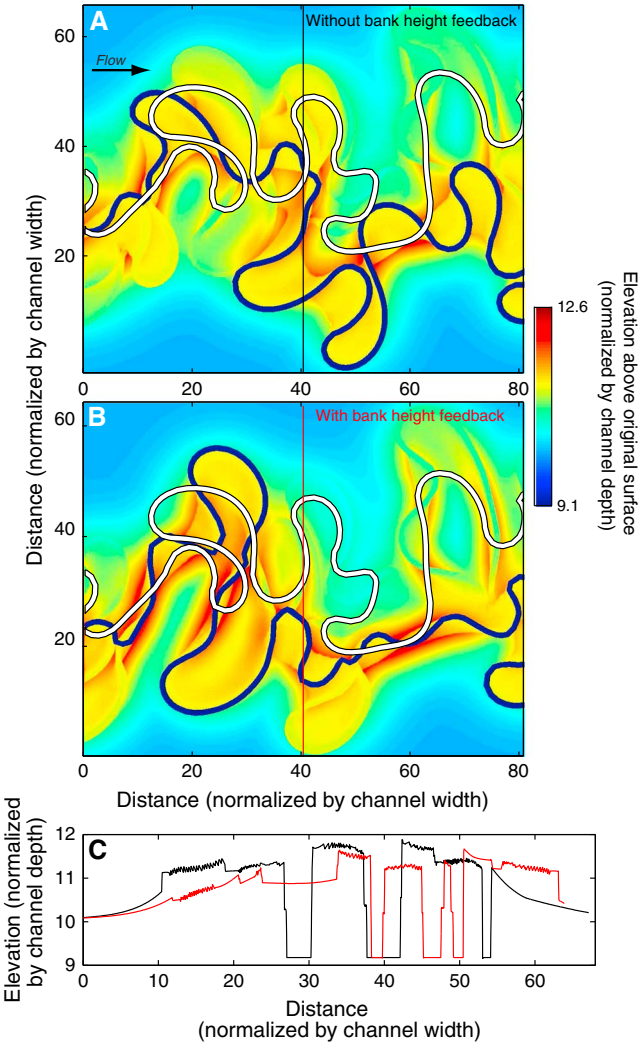

Figure 8. Simulated landscapes formed by channel migration and floodplain deposition. Elevation above the original surface is normalized by channel depth; distance is normalized by channel width. Sediment accumulates by overbank deposition, with constant and exponential decay terms (equation (10)). Simulation parameters are a maximum lateral erosion rate of 1 m/yr, η =10 mm/yr, D_s = 3 mm/yr, and λ = 4w. Arrow indicates general flow direction. The white trace indicates initial channel planform geometry; the active channel is in dark blue. (a and b) Topographic profiles run from top to bottom. Figure 8a shows topography when channel lateral migration rate is insensitive to bank height. Figure 8b shows topography when channel lateral migration rate varies inversely with bank height. (c) Topographic profiles for the case without the bank height feedback (black) and with the feedback (red).

of the channel, it is also flexible to reconstruct floodplain topography due to overbank deposition—even though floodplain elevations are not explicitly stored in memory during the simulation (see section 4). Moreover, unlike a grid-based formulation for tracking topography, which applies the same overbank deposition rate across the area of an entire grid cell, the vector-based approach allows calculation of the exact local elevation during the simulation and hence more precise topographic tracking. Such precise tracking is needed when, for example, local differences in bank height alter channel lateral migration rates (equation (12)) or the quantity of sediment entrained from the eroding bank [e.g., *Parker et al.*, 2011].

6. Discussion

[53] Model results using the grid- and vector-based bank-material tracking schemes should converge in the limit of high grid resolution (equation (7)), because when the grid cells are small enough to record all bank migration, there is no threshold for updating bank-material properties. To assess the degree to which grid-based model predictions approach a vector-based prediction as grid resolution increases, we analyze the landscape area altered by bank migration in each time step using the channel trajectory from Figures 5a–5c. Figure 9 shows the mean bank area updated in each time step using grids of different resolutions, normalized by the value for the vector-based approach. These simulations demonstrate that the mean area updated using the grid-based approach asymptotes to the value for the vector-based approach when small nondimensional grid resolutions are computationally feasible.

[54] The case studies presented herein demonstrate that a framework that couples meandering to bank-material evolution is free of resolution dependence when the active channel bank and the topography itself are represented in vector form. Given memory constraints which limit the practical resolution of grid-based methods, the vector-based framework is advantageous in landscapes with high variability in bank strength, which may occur in depositional environments with variable grain sizes and in net-erosional landscapes with mixed bedrock and sediment banks. Simulations show the new framework to be flexible to track meander belt topographic (Figures 5 and 8) and stratigraphic evolution (Figure 6), and channel incision (Figure 7). Phenomena not discussed here—such as asymmetric channel cross sections and overbank

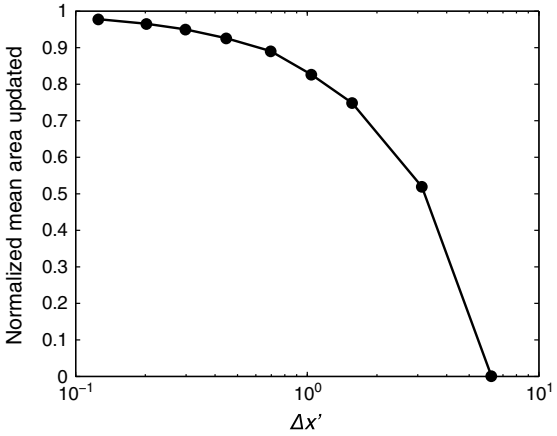

Figure 9. Bank area updated for the same channel trajectory as in Figures 5a–5c but with variable grid resolution. The mean area updated by the channel banks in a single time step, normalized by the value for vector-based bank material tracking, is plotted for a range of nondimensional grid cell widths ($\Delta x' = \Delta x/(E_L \Delta t)$). The finest resolution corresponds to a dimensional cell width of 0.5 m. The area updated asymptotes to the value obtained using vector-based bank-material tracking.

deposition with different grain sizes—could also be incorporated using vector-based techniques.

[55] Bank migration simulations involving grids are more likely to be resolution independent for cases of constant bank resistance and for cases where the characteristic bank migration distance in one time step is larger than the cell width. In the vector-based scheme presented here, bank-material properties are determined by computations based on stored data (e.g., interpolation of past channel longitudinal profiles to determine elevation). In contrast, when the memory cost is feasible, grid-based frameworks eliminate some computation time because bank-material properties are directly accessed. Therefore in cases, computation time may be an important subsidiary consideration in selecting a method for bank-material tracking, particularly when algorithms for reconstructing erodibility are complex.

[56] The traditional grid-based approach remains efficient for sediment routing approaches to modeling fluvial systems [*Coulthard and Van De Wiel*, 2006; *Karssenberg and Bridge*, 2008], particularly those dominated by braiding [*Murray and Paola*, 1994], in which channel banks are ephemeral. Consequently, connecting vector-based and grid-based frameworks for topographic representation may represent an important next step in advancing landscape evolution modeling for meandering channels. In such a framework, grid elements could continue to represent hillslopes as in current landscape evolution models [e.g., *Tucker et al*., 2001] and to route sediment within active channels. Vector elements would be used to track sharp discontinuities in elevation or bank-material composition related to channel migration, as presented here, as well as drainage divides because their precise locations are often between grid nodes [*Castelltort et al*., 2012]. The cut-cell method [*Beyer and LeVeque*, 1992], which temporarily slices cells crossed by a boundary, could also be used with an Eulerian grid to represent hillslopes. In this way, an extended time series of bank advance could be used to create a complex valley boundary shape within a rectangular grid [*Udaykumar and Shyy*, 1995; *Udaykumar et al*., 1996, 1999]. As with using an adaptive mesh to track moving boundaries, however, using the cut-cell technique could be computationally intensive [*Udaykumar et al*., 1999]—in this case because sediment fluxes would have to be tracked across cells with complicated geometries.

[57] Although the examples explored here only involve river channels, the vector-based framework for bank-material tracking could be applied to any environment in which bank-material properties interact with a channel. Potential applications include channels formed by sediment in tidal, deltaic, and submarine environments; and channels in which thermodynamic processes are important. For example, channels formed by lava and supraglacial channels evolve largely based on heat fluxes, which determine the spatial distribution of freezing and melting [*Parker*, 1975; *Kerr*, 2001; *Karlstrom et al*., 2013]. As these channels migrate, they may reset the local temperature field, just as river channels alter topography as they migrate, which implies interaction between channel migration and bank-material properties. Vector-based channel extent tracking could be useful for recording the kinematics of these channels.

[58] The similarities between subaerial rivers and submarine channels formed by turbidity currents suggest more direct applications of the present framework. In deposits formed by submarine channels, the spatial distribution of grain size is determined by channel migration and aggradation [*Sylvester et al*., 2011]. Cohesive fine-grained sediments [*Panagiotopoulos et al*., 1997] may inhibit channel migration, as suggested for clay plugs in subaerial oxbows [*Fisk*, 1947; *Allen*, 1982; *Ikeda*, 1989]. While grid-based methods exist for tracking stratigraphy formed by meandering channels [e.g., *Clevis et al*., 2006], such methods would be susceptible to grid resolution-scale erosion thresholds. Therefore, the vector-based approach could advance modeling of channel-bank interactions for stratigraphic development.

7. Conclusions

[59] Grid-based models are commonly applied to representing the evolution of bank-material properties in environments shaped by channel migration. However, simulation results are highly resolution dependent when there are large differences in bank strength and when the characteristic bank migration distance is less than one grid cell width. We have developed a new, vector-based framework for representing bank-material properties that extends existing vector-based approaches and does not have the problem of resolution dependence found in grid-based techniques. For areas the channel has migrated across, bank-material properties are reconstructed using vector-based channel geometric data. This approach can treat sloping longitudinal profiles, overbank deposition, and stratigraphic development and may be adapted to a variety of environments in which channel migration interacts with topography or stratigraphy. This enables more accurate modeling of the coevolution of channels and bank-material properties, particularly where there are large contrasts in bank strength.

[60] Case studies show that erodibility differences due to bank-material properties or bank height can strongly influence the coevolution of channels and the surrounding topography and stratigraphy. Oxbow-filling sediments that are less erodible than other floodplain sediments can narrow the width of meander belts and stacked channel deposits; grid-based methods may artificially enhance this narrowing effect if the grid resolution is coarse. A simulation of meandering river evolution in a bedrock valley indicates that meandering kinematics and patterns of valley widening respond strongly to bank strength differences between bedrock and sediment; grid-based methods can artificially restrict valley widening by implicitly imposing a threshold to update bank properties. Finally, simulations suggest that elevation differences due to spatial variations in overbank deposition across a floodplain strongly influence channel trajectory and floodplain topography when the channel lateral migration rate responds to bank height.

[61] **Acknowledgments.** This work was supported by the Department of Defense through the National Defense Science and Engineering Graduate Fellowship (NDSEG) Program and NSF grant EAR-1147381 to MPL. We thank Noah Finnegan, Antoine Lucas, Edwin Kite, and Vamsi Ganti for helpful discussions and Nicole Gasparini and three anonymous reviewers for their valuable comments.

References

Abreu, V., M. Sullivan, C. Pirmez, and D. Mohrig (2003), Lateral accretion packages (LAPs): An important reservoir element in deep water sinuous channels, *Mar. Pet. Geol.*, *20*(6–8), 631–648, doi:10.1016/j.marpetgeo.2003.08.003.

Allen, J. R. (1982), Free meandering channels and lateral deposits, in *Sedimentary Structures, Their Character and Physical Basis*, vol. 2, pp. 53–100, Elsevier Science and Technology, New York.

Beyer, R. P., and R. J. LeVeque (1992), Analysis of a one-dimensional model for the immersed boundary method, *SIAM J. Numer. Anal.*, *29*(2), 332–364.

Blondeaux, P., and G. Seminara (1985), A unified bar-bend theory of river meanders, *J. Fluid Mech.*, *157*, 449–470.

Blum, M. D., and T. E. Tornqvist (2000), Fluvial responses to climate and sea-level change: A review and look forward, *Sedimentology*, *47*, 2–48, doi:10.1046/j.1365-3091.2000.00008.x.

Braudrick, C. A., W. E. Dietrich, G. T. Leverich, and L. S. Sklar (2009), Experimental evidence for the conditions necessary to sustain meandering in coarse-bedded rivers, *Proc. Natl. Acad. Sci. U. S. A.*, *106*(40), 16,936–16,941, doi:10.1073/pnas.0909417106.

Bridge, J. S. (2003), *Rivers and Floodplains: Forms, Processes, and Sedimentary Record*, Wiley-Blackwell, Malden, Massachusetts.

Burr, D. M., J. T. Perron, M. P. Lamb, R. P. Irwin, G. C. Collins, A. D. Howard, L. S. Sklar, J. M. Moore, M. Ádámkovics, and V. R. Baker (2013), Fluvial features on Titan: Insights from morphology and modeling, *Geol. Soc. Am. Bull.*, *125*(3–4), 299–321, doi:10.1130/B30612.1.

Camporeale, C., P. Perona, A. Porporato, and L. Ridolfi (2005), On the long-term behavior of meandering rivers, *Water Resour. Res.*, *41*, W12403, doi:10.1029/2005WR004109.

Castelltort, S., L. Goren, S. D. Willett, J.-D. Champagnac, F. Herman, and J. Braun (2012), River drainage patterns in the New Zealand Alps primarily controlled by plate tectonic strain, *Nat. Geosci.*, *5*(10), 744–748, doi:10.1038/ngeo1582.

Clevis, Q., G. E. Tucker, G. Lock, S. T. Lancaster, N. Gasparini, A. Desitter, and R. L. Bras (2006), Geoarchaeological simulation of meandering river deposits and settlement distributions: A three-dimensional approach, *Geoarchaeology*, *21*(8), 843–874, doi:10.1002/gea.20142.

Constantine, J. A., and T. Dunne (2008), Meander cutoff and the controls on the production of oxbow lakes, *Geology*, *36*(1), 23–26, doi:10.1130/G24130A.1.

Coulthard, T. J., and M. J. Van De Wiel (2006), A cellular model of river meandering, *Earth Surf. Processes Landforms*, *31*(1), 123–132, doi:10.1002/esp.1315.

Crosato, A. (2007), Effects of smoothing and regridding in numerical meander migration models, *Water Resour. Res.*, *43*, W01401, doi:10.1029/2006WR005087.

Darby, S. E. (2002), Numerical simulation of bank erosion and channel migration in meandering rivers, *Water Resour. Res.*, *38*(9), 1163, doi:10.1029/2001WR000602.

Davies, N. S., and M. R. Gibling (2010), Paleozoic vegetation and the Siluro-Devonian rise of fluvial lateral accretion sets, *Geology*, *38*(1), 51–54, doi:10.1130/G30443.1.

Dietrich, W. E., and J. T. Perron (2006), The search for a topographic signature of life, *Nature*, *439*(7075), 411–418, doi:10.1038/nature04452.

Dietrich, W. E., D. G. Bellugi, L. S. Sklar, J. D. Stock, A. M. Heimsath, and J. J. Roering (2003), Geomorphic transport laws for predicting landscape form and dynamics, in *Geophysical Monograph Series*, vol. 135, edited by P. R. Wilcock and R. M. Iverson, pp. 103–132, AGU, Washington, D. C.

Duan, J. G., and P. Y. Julien (2010), Numerical simulation of meandering evolution, *J. Hydrol.*, *391*(1–2), 34–46, doi:10.1016/j.jhydrol.2010.07.005.

Fagherazzi, S., A. Bortoluzzi, W. E. Dietrich, A. Adami, S. Lanzoni, M. Marani, and A. Rinaldo (1999), Tidal networks 1. Automatic network extraction and preliminary scaling features from digital terrain maps, *Water Resour. Res.*, *35*(12), 3891–3904.

Finnegan, N. J., and W. E. Dietrich (2011), Episodic bedrock strath terrace formation due to meander migration and cutoff, *Geology*, *39*(2), 143–146, doi:10.1130/G31716.1.

Finnegan, N. J., G. Roe, D. R. Montgomery, and B. Hallet (2005), Controls on the channel width of rivers: Implications for modeling fluvial incision of bedrock, *Geology*, *33*(3), 229–232, doi:10.1130/G21171.1.

Fisk, H. N. (1947), *Fine-Grained Alluvial Deposits and Their Effect on Mississippi River Activity*, Waterways Experiment Station US Army Corps of Engineers, Vicksburg.

Fuller, T. K., L. A. Perg, J. K. Willenbring, and K. Lepper (2009), Field evidence for climate-driven changes in sediment supply leading to strath terrace formation, *Geology*, *37*(5), 467–470.

Greeley, R., S. A. Fagents, R. S. Harris, S. D. Kadel, D. A. Williams, and J. E. Guest (1998), Erosion by flowing lava: Field evidence, *J. Geophys. Res.*, *103*(B11), 27,325–27,345, doi:10.1029/97JB03543.

Güneralp, İ., and B. L. Rhoads (2011), Influence of floodplain erosional heterogeneity on planform complexity of meandering rivers, *Geophys. Res. Lett.*, *38*, L14401, doi:10.1029/2011GL048134.

Hajek, E. A., P. L. Heller, and B. A. Sheets (2010), Significance of channel-belt clustering in alluvial basins, *Geology*, *38*(6), 535–538.

Hancock, G. S., and R. S. Anderson (2002), Numerical modeling of fluvial strath-terrace formation in response to oscillating climate, *Geol. Soc. Am. Bull.*, *114*(9), 1131–1142.

Harden, D. (1990), Controlling factors in the distribution and development of incised meanders in the central Colorado Plateau, *Geol. Soc. Am. Bull.*, *102*(2), 233–242, doi:10.1130/0016-7606(1990)102<0233:CFITDA>2.3.CO;2.

Henriquez, A., K. Tyler, and A. Hurst (1990), Characterization of fluvial sedimentology for reservoir simulation modeling, *SPE Form. Eval.*, *5*(3), 211–216, doi:10.2118/18323-PA.

Hirst, J. P. P., C. R. Blackstock, and S. Tyson (1993), Stochastic modeling of fluvial sandstone bodies, in *The Geological Modeling of Hydrocarbon Reservoirs and Outcrop Analogues: International Association of Sedimentologists*, Special Publication, vol. 15, edited by S. S. Flint and I. D. Bryant, pp. 237–252, Blackwell, Oxford, UK.

Howard, A. D. (1984), Simulation model of meandering, in *River Meandering*, edited by C. Elliot, pp. 952–963, ASCE, New York.

Howard, A. D. (1992), Modeling channel migration and floodplain sedimentation in meandering streams, in *Lowland Floodplain Rivers: Geomorphological Perspectives*, edited by P. A. Carling and G. E. Petts, pp. 1–41, John Wiley, Ltd., Chichester.

Howard, A. D. (1996), Modeling channel evolution and floodplain morphology, in *Floodplain Processes*, edited by M. G. Anderson, D. E. Walling, and P. E. Bates, pp. 15–62, John Wiley, Ltd., Chichester.

Howard, A., and A. Hemberger (1991), Multivariate characterization of meandering, *Geomorphology*, *4*(3–4), 161–186, doi:10.1016/0169-555X(91)90002-R.

Howard, A. D., and G. Kerby (1983), Channel changes in badlands, *Geol. Soc. Am. Bull.*, *94*(6), 739–752.

Howard, A. D., and T. R. Knutson (1984), Sufficient conditions for river meandering—A simulation approach, *Water Resour. Res.*, *20*(11), 1659–1667, doi:10.1029/WR020i011p01659.

Hudson, P. F., and R. H. Kesel (2000), Channel migration and meander-bend curvature in the lower Mississippi River prior to major human modification, *Geology*, *28*(6), 531, doi:10.1130/0091-7613(2000)28<531:CMAMCI>2.0.CO;2.

Ikeda, H. (1989), Sedimentary controls on channel migration and origin of point bars in sand-bedded meandering rivers, *Water Resour. Monogr.*, *12*, 51–68, doi:10.1029/WM012p0051.

Ikeda, S., G. Parker, and K. Sawai (1981), Bend theory of river meanders. Part 1. Linear development, *J. Fluid Mech.*, *112*(11), 363–377.

Johannesson, H., and G. Parker (1989), Linear theory of river meanders, *Water Resour. Monogr.*, *12*, 181–213, doi:10.1029/WM012p0181.

Karlstrom, L., P. Gajjar, and M. Manga (2013), Meander formation in supraglacial streams, *J. Geophys. Res. Earth Surface*, *118*, 1897–1907, doi:10.1002/jgrf.20135.

Karssenberg, D., and J. S. Bridge (2008), A three-dimensional numerical model of sediment transport, erosion and deposition within a network of channel belts, floodplain and hill slope: Extrinsic and intrinsic controls on floodplain dynamics and alluvial architecture, *Sedimentology*, *55*(6), 1717–1745.

Katsikadelis, J. T. (2002), *Boundary Elements: Theory and Applications*, Elsevier, Kidlington, Oxford.

Kerr, R. C. (2001), Thermal erosion by laminar lava flows, *J. Geophys. Res.*, *106*(B11), 26,453–26,465.

Komatsu, G., and V. R. Baker (1996), Channels in the solar system, *Planet. Space Sci.*, *44*(8), 801–815, doi:10.1016/0032-0633(96)00010-4.

Kondolf, G. M. (2006), River restoration and meanders, *Ecol.Soc.*, *11*(2), 42.

Lancaster, S. T. (1998), A nonlinear river meandering model and its incorporation in a landscape evolution model, PhD thesis, Massachusetts Institute of Technology, Cambridge, Massachusetts.

Lancaster, S. T., and R. L. Bras (2002), A simple model of river meandering and its comparison to natural channels, *Hydrol. Processes*, *16*(1), 1–26, doi:10.1002/hyp.273.

Leopold, L. B., and M. G. Wolman (1957), *River Channel Patterns: Braided, Meandering, and Straight*, U.S. Govt. Printing Office, Washington, D. C.

Lewin, J. (1976), Initiation of bed forms and meanders in coarse-grained sediment, *Geol. Soc. Am. Bull.*, *87*(2), 281–285, doi:10.1130/0016-7606(1976)87<281:IOBFAM>2.0.CO;2.

Lewin, J., and B. J. Brindle (1977), Confined meanders, in *River Channel Changes*, edited by K. J. Gregory, pp. 221–233, John Wiley, Chichester.

Li, S., and W. K. Liu (2002), Meshfree and particle methods and their applications, *Appl. Mech. Rev.*, *55*(1), 1–34.

Liu, G. R. (2010), *Meshfree Methods: Moving Beyond the Finite Element Method*, CRC Press, Washington, D. C.

Montgomery, D. R. (2004), Observations on the role of lithology in strath terrace formation and bedrock channel width, *Am. J. Sci.*, *304*(5), 454–476, doi:10.2475/ajs.304.5.454.

Motta, D., J. D. Abad, E. J. Langendoen, and M. H. Garcia (2012a), A simplified 2D model for meander migration with physically-based bank evolution, *Geomorphology*, *163*, 10–25.

Motta, D., J. D. Abad, E. J. Langendoen, and M. H. García (2012b), The effects of floodplain soil heterogeneity on meander planform shape, *Water Resour. Res.*, *48*, W09518, doi:10.1029/2011WR011601.

Murray, A. B., and C. Paola (1994), A cellular model of braided rivers, *Nature*, *371*, 54–57.

Nagata, N., T. Hosoda, and Y. Muramoto (2000), Numerical analysis of river channel processes with bank erosion, *J. Hydraul. Eng.*, *126*(4), 243–252, doi:10.1061/(ASCE)0733-9429(2000)126:4(243).

Nanson, G. C., and E. J. Hickin (1983), Channel migration and incision on the Beatton River, *J. Hydraul. Eng.*, *109*(3), 327–337.

Nicoll, T. J., and E. J. Hickin (2010), Planform geometry and channel migration of confined meandering rivers on the Canadian prairies, *Geomorphology*, *116*(1–2), 37–47, doi:10.1016/j.geomorph.2009.10.005.

Osman, A., and C. Thorne (1988), Riverbank stability analysis. I: Theory, *J. Hydraul. Eng.*, *114*(2), 134–150, doi:10.1061/(ASCE)0733-9429(1988)114:2(134).

Panagiotopoulos, I., G. Voulgaris, and M. B. Collins (1997), The influence of clay on the threshold of movement of fine sandy beds, *Coastal Eng.*, *32*(1), 19–43, doi:10.1016/S0378-3839(97)00013-6.

Parker, G. (1975), Meandering of supraglacial melt streams, *Water Resour. Res.*, *11*(4), 551–552, doi:10.1029/WR011i004p00551.

Parker, G., P. Diplas, and J. Akiyama (1983), Meander bends of high amplitude, *J. Hydraul. Eng.*, *109*(10), 1323–1337, doi:10.1061/(ASCE)0733-9429(1983)109:10(1323).

Parker, G., Y. Shimizu, G. V. Wilkerson, E. C. Eke, J. D. Abad, J. W. Lauer, C. Paola, W. E. Dietrich, and V. R. Voller (2011), A new framework for modeling the migration of meandering rivers, *Earth Surf. Processes Landforms*, *36*(1), 70–86, doi:10.1002/esp.2113.

Posner, A. J., and J. G. Duan (2012), Simulating river meandering processes using stochastic bank erosion coefficient, *Geomorphology*, *163–164*, 26–36, doi:10.1016/j.geomorph.2011.05.025.

Pyrcz, M. J., and C. V. Deutsch (2005), Conditioning event-based fluvial models, in *Geostatistics Banff 2004*, vol. 14, pp. 135–144, Springer, Netherlands.

Pyrcz, M. J., J. B. Boisvert, and C. V. Deutsch (2009), ALLUVSIM: A program for event-based stochastic modeling of fluvial depositional systems, *Comput. Geosci.*, *35*(8), 1671–1685, doi:10.1016/j.cageo.2008.09.012.

Seminara, G. (2006), Meanders, *J. Fluid Mech.*, *554*(1), 271–297, doi:10.1017/S0022112006008925.

Shimizu, Y. (2002), A method for simultaneous computation of bed and bank deformation of a river, in *River Flow 2002*, vol. 2, edited by D. Bousmar and Y. Zech, pp. 793–801, Taylor and Francis, London.

Shiono, K., Y. Muto, D. W. Knight, and A. F. L. Hyde (1999), Energy losses due to secondary flow and turbulence in meandering channels with overbank flows, *J. Hydraul. Res.*, *37*(5), 641–664, doi:10.1080/00221689909498521.

Smith, C. D. (1978), Effect of channel meanders on flood stage in valley, *J. Hydraul. Div.*, *104*(1), 49–58.

Stark, C. P., J. R. Barbour, Y. S. Hayakawa, T. Hattanji, N. Hovius, H. Chen, C.-W. Lin, M.-J. Horng, K.-Q. Xu, and Y. Fukahata (2010), The climatic signature of incised river meanders, *Science*, *327*(5972), 1497–1501, doi:10.1126/science.1184406.

Stølum, H.-H. (1996), River meandering as a self-organization process, *Science*, *271*(5256), 1710–1713, doi:10.1126/science.271.5256.1710.

Sun, T., P. Meakin, T. Jossang, and K. Schwarz (1996), A simulation model for meandering rivers, *Water Resour. Res.*, *32*(9), 2937–2954, doi:10.1029/96WR00998.

Sun, T., P. Meakin, and T. Jøssang (2001), A computer model for meandering rivers with multiple bed load sediment sizes: 2 Computer simulations, *Water Resour. Res.*, *37*(8), 2243–2258.

Sylvester, Z., C. Pirmez, and A. Cantelli (2011), A model of submarine channel-levee evolution based on channel trajectories: Implications for stratigraphic architecture, *Mar. Pet. Geol.*, *28*(3), 716–727, doi:10.1016/j.marpetgeo.2010.05.012.

Thorne, C. R. (1992), Bend scour and bank erosion on the meandering Red River, Louisiana, in *Lowland Floodplain Rivers: Geomorphological Perspectives*, pp. 95–115, John Wiley, Chichester.

Trush, W. J., S. M. McBain, and L. B. Leopold (2000), Attributes of an alluvial river and their relation to water policy and management, *Proc. Natl. Acad. Sci. U. S. A.*, *97*(22), 11,858–11,863, doi:10.1073/pnas.97.22.11858.

Tucker, G. E., and G. R. Hancock (2010), Modeling landscape evolution, *Earth Surf. Processes Landforms*, *35*(1), 28–50, doi:10.1002/esp.1952.

Tucker, G. E., S. T. Lancaster, N. M. Gasparini, and R. L. Bras (2001), The channel-hillslope integrated landscape development model (CHILD), in *Landscape Erosion and Evolution Modeling*, edited by R. S. Harmon and W. W. Doe III, pp. 349–388, Kluwer Academic/Plenum Publishers, New York.

Turowski, J. M., N. Hovius, H. Meng-Long, D. Lague, and C. Men-Chiang (2008), Distribution of erosion across bedrock channels, *Earth Surf. Processes Landforms*, *33*(3), 353–363, doi:10.1002/esp.1559.

Udaykumar, H. S., and W. Shyy (1995), Simulation of interfacial instabilities during solidification—I Conduction and capillarity effects, *Int. J. Heat Mass Transfer*, *38*(11), 2057–2073, doi:10.1016/0017-9310(94)00315-M.

Udaykumar, H. S., W. Shyy, and M. M. Rao (1996), Elafint: A mixed Eulerian-Lagrangian method for fluid flows with complex and moving boundaries, *Int. J. Numer. Methods Fluids*, *22*(8), 691–712, doi:10.1002/(SICI)1097-0363(19960430)22:8<691::AID-FLD371>3.0.CO;2-U.

Udaykumar, H. S., R. Mittal, and W. Shyy (1999), Computation of solid-liquid phase fronts in the sharp interface limit on fixed grids, *J. Comput. Phys.*, *153*(2), 535–574, doi:10.1006/jcph.1999.6294.

Van De Wiel, M. J., T. J. Coulthard, M. G. Macklin, and J. Lewin (2011), Modeling the response of river systems to environmental change: Progress, problems and prospects for palaeo-environmental reconstructions, *Earth Sci. Rev.*, *104*(1–3), 167–185, doi:10.1016/j.earscirev.2010.10.004.

Weertman, J. (1972), General theory of water flow at the base of a glacier or ice sheet, *Rev. Geophys.*, *10*(1), 287–333, doi:10.1029/RG010i001p00287.

Whipple, K. X. (2004), Bedrock rivers and the geomorphology of active orogens, *Annu. Rev. Earth Planet. Sci.*, *32*(1), 151–185, doi:10.1146/annurev.earth.32.101802.120356.

Wobus, C. W., G. E. Tucker, and R. S. Anderson (2006), Self-formed bedrock channels, *Geophys. Res. Lett.*, *33*, L18408, doi:10.1029/2006GL027182.

Yanites, B. J., and G. E. Tucker (2010), Controls and limits on bedrock channel geometry, *J. Geophys. Res.*, *115*, F04019, doi:10.1029/2009JF001601.

Zolezzi, G., and G. Seminara (2001), Downstream and upstream influence in river meandering. Part 1. General theory and application to overdeepening, *J. Fluid Mech.*, *438*, 183–211.